SLAC–PUB–5761
March 1992
T/E

The Space-Time Structure of Deep Inelastic Lepton-Hadron Scattering*

VITTORIO DEL DUCA AND STANLEY J. BRODSKY

Stanford Linear Accelerator Center

Stanford University, Stanford, California 94309

and

PAUL HOYER

Department of Physics

University of Helsinki, Helsinki, Finland

Submitted to *Physical Review D*

* Work supported by the Department of Energy, contract DE–AC03–76SF00515.

ABSTRACT

We discuss the space-time structure of deep inelastic scattering in the target rest frame. At small x_{bj}, the process is dominated by quark pair production, and the "Ioffe time" between the production of the pair and its interaction in the target is long. We compute the leading logarithmic corrections to the parton model predictions for the virtual photo-absorption cross section, and analyze the transverse size of the pair and the Ioffe time as a function of the dynamical variables of the pair constituents. Both the transverse size and the Ioffe time depend significantly on the polarization (longitudinal or transverse) of the virtual photon. Hence one may expect that nuclear scattering corrections, including shadowing, may also be polarization dependent.

1. Introduction

Despite 20 years of progress in testing quantum chromodynamics, a fundamental understanding of the physical mechanisms that connect the underlying quark and gluon scattering subprocesses of QCD to the observed final state hadrons remains elusive. It is now recognized that experiments using nuclear targets and beams provide a unique tool for probing hadronization, since the nuclear medium itself can physically modify the hadronization process. For example, in deep inelastic lepto-production $\ell p \to \ell H X$, the presence of a nucleus in the final state will lead to transverse momentum smearing and induced elastic and inelastic energy loss of the produced hadrons, as well as influence the color fields and color screening of the outgoing quark-jet system. The postulate that the process of hadron creation has an intrinsic formation time τ_H implies that at high energies $\nu > M_N R_A/\tau_H$ the quark and gluon precursors, rather than the final state hadrons, scatter in the nucleus. Furthermore, since the nucleus is transparent to small color-singlet states, it can act as a color filter, differentiating production mechanisms for processes such as large momentum quasi-elastic scattering and heavy quarkonium production. The nucleus is thus an essential instrument for resolving the space-time structure of fundamental QCD processes at fermi-size scales.

The simplest experiment for analyzing and controlling the effects of a nuclear medium on QCD processes is deep inelastic lepton scattering (DIS) on a nuclear target. It is traditional to analyze the space-time structure of DIS from the standpoint of the target's infinite momentum frame (or, equivalently, at fixed light-cone time), since in that frame the current is essentially trivial and the physics of the DIS structure functions can be identified with the quark distributions of the target;

e.g.,

$$F_2(x,Q^2) = \sum_{q,\bar{q}} e_q^2 x G_{q/p}(x,Q^2) \tag{1.1}$$

(see Fig. 1). However, the simplicity of this description becomes lost when one considers nuclear target effects, since the physics of the nucleus is essentially unknown in the $P_z \to \infty$ frame. The wealth of knowledge one has from nuclear physics on nucleon wavefunctions, meson exchange currents, etc. strictly pertains to the nuclear rest frame; the relativistic boost of a nuclear wavefunction requires a fundamental understanding of the internal nuclear dynamics [1] .

Thus, in order to utilize the nucleus as a probe of QCD processes, rather than study the structure of the nucleus itself, it is mandatory that the space-time structure of DIS be analyzed in the target rest frame. Unfortunately, much of the simplicity of the parton model description of Bjorken-scaling becomes lost in the target rest frame, since in general one must consider time-ordered processes where the virtual photon creates pairs (as in Fig. 2a) or scatters on vacuum fluctuations (as in Fig. 2b), as well as scattering on the quark constituents already present in the target wavefunction (Fig. 2c). In the limit of large photon energy $\nu = q\cdot p/M_N$, the dominant time-ordered process in the lab frame is virtual $q\bar{q}$ pair production (as in Fig. 2a) where one of the quarks of the pair scatters, annihilates, or is captured in the target. Thus at high ν in the lab frame, the physics of DIS is dominated by the Fock state structure of the virtual photon, rather than that of the target. In fact, it is natural to identify sea quark and heavy quark contributions to the deep inelastic structure functions at small $x_{Bj} = Q^2/2q\cdot p$ with Bethe-Heitler pair production processes such as that shown in Fig. 3. The presence of spin-one gluon exchange in the t-channel automatically implies constant photo-absorption

cross sections at high ν and thus non-vanishing structure functions $F_2(x_{bj}, Q^2)$ at $x_{bj} \to 0$. Alternatively, one can identify this type of pair production process with the photon-gluon fusion mechanism or the evolution of the proton structure functions and its related radiative corrections. However, from the standpoint of physics in the rest frame, it is most natural to identify pair production at high ν as the materialization of the photon's hadronic structure by the proton target.[1]

Of course, the frame dependence of DIS does not arise in a strictly Lorentz-invariant description of DIS, as in the covariant parton model of Landshoff, Polkinghorne and Short [3] . However, a space-time description requires a fixed-time Hamiltonian formalism. In the next section we show how a covariant framework can be used to relate the physics and kinematics of DIS quantized at fixed time in the target rest frame to the kinematics of the light-cone formalism.

One of the most important concepts in the analysis of the spacetime structure of DIS in the target rest frame is the Ioffe time τ_I [4] , which is defined as the effective distance between the production of the quark pair and its interaction in the nucleus. The virtuality of the pair $\mathcal{M}^2 = \mathcal{O}(Q^2)$ in the Bjorken scaling region, implies that

$$\tau_I = \frac{C_I}{x_{bj} M_N}, \tag{1.2}$$

where $C_I = \mathcal{O}(1)$ is a characteristic dimensionless constant. Thus for small x_{bj} the photon converts to a quark pair at a large distance before it interacts in the target; for example, at HERA where one can study structure functions at $x_{bj} \sim 10^{-5}$ the

1 For example, by using the target rest frame picture, it is easy to see that the pair production process of Fig. 2a on a proton target will generally lead to breaking of isospin symmetry of the anti-quark sea $\overline{d}(x) \neq \overline{u}(x)$ because of the stronger Pauli-blocking by the u quarks already present in the proton wavefunction. This type of isospin breaking could account for the observed violation of the Gottfried sum rule [2] .

Ioffe distance is as large as 10^4 fm, much larger than nuclear radii. At lower values of x_{bj}, pair production can occur within the nuclear volume, thus reducing the total nuclear path length.

As we shall show in this paper, the constant C_I in the Ioffe time has an essential dependence on the polarization of the virtual photon. Thus in a given experiment, one can control the Ioffe time and its consequences for nuclear effects, not only by choosing x_{bj} but also by selecting longitudinal versus transverse photons.

As a working model for nuclear effects, we visualize the following physical picture for the space-time structure of deep inelastic scattering in a nuclear target in the target rest frame. (See Fig. 4.)

1. The virtual photon creates a virtual $q\overline{q}$ pair of invariant mass of order Q. The gluons g_1, g_2, g_3 radiated near the vertex are associated with the QCD evolution and radiative corrections to the quark structure function.

2. The pair propagates over the Ioffe time, and then the member of the pair with the least energy (shown as a $\overline{q}$ in Fig. 4) gives the main interaction in the nucleus. The propagation of this quark or antiquark through the nuclear medium can be described by the Glauber multiple scattering theory [5] used for hadron-nucleus interactions. For example, the elastic scattering of the $\overline{q}$ on upstream nucleons such as N_1 in Fig. 4 before interacting inelastically on nucleon N_2 reduces the flux of $\overline{q}$ reaching N_2. A model of shadowing (and anti-shadowing) of the nuclear DIS cross section based on this description is given in Ref. [6] .

3. The other member of the pair (the q in Fig. 4) carries the majority of the photon energy; its hadronization provides the usual "current quark" jet. However, during its transit through the nucleus this quark could scatter on

nucleons such as N_3, thus broadening the transverse momentum distribution of the produced hadrons. The quark can also scatter inelastically and lose energy by nuclear-induced radiation, as shown, for example, by the emission of gluon g_4. The Landau-Pomeranchuk-Feinberg formation zone analysis [7] however shows the induced energy loss is finite in the laboratory frame and does not scale with ν. (As shown in Ref. [8] this can be understood as due to the destructive interference at low momentum transfer of the amplitudes producing g_4 from nucleons N_3 or N_4.) Since the induced k_t broadening conserves probability, the hadron distribution integrated over transverse momentum is unchanged. Furthermore, since the induced energy loss is negligible compared to the scale ν, this effect does not disturb leading-twist QCD factorization. Thus the fragmentation function $D_H(z, Q^2)$ with $z = p \cdot p_H / p \cdot q$, is independent of the nuclear medium; any nuclear dependent-energy loss is only expected at low ν.

4. Finally hadronization of the separated 3 and $\overline{3}$ jets occur. However, because of the presence of the nuclear medium the resulting hadrons will have a broadened transverse momentum distribution $\langle k_t^2 \rangle_A$ and a finite energy loss $\langle \Delta E_H \rangle_A$ in proportion to the path length of the leading current quark through the nucleus which, in turn, depends on the Ioffe time. As we have noted, one can control the Ioffe time and its consequences for nuclear effects, not only by choosing x_{bj}, but also by selecting the polarization of the virtual photon.

We also note that induced electromagnetic radiation caused by the transit of the current quark through the nucleus should also increase with Ioffe time. Thus the nuclear dependence of associated soft photons in DIS as a function of x_{bj} and

virtual photon polarization will provide important tests of the space-time picture presented here. In addition, the absolute magnitude of the nuclear dependent photon radiation could provide a value for the quark-nucleon cross section.

In this paper we will present a detailed calculation of the basic size parameters controlling DIS including the Ioffe time and the impact separation of the pair. The model we use, as in the paper of Bjorken, Kogut, and Soper [9] , corresponds to Bethe-Heitler pair production by the virtual photon in the Coulomb field of a target nucleon. The vector exchange allows a non-vanishing of the structure functions at low x_{bj}. A similar model but with finite gluon mass has also been analyzed in Ref. [10] . As emphasized by Bjorken, the special kinematic region of asymmetric pairs (where one quark carries only finite laboratory momentum) plays a special role in the analysis. In this kinematic regime, the low momentum quark or anti-quark can equally well be identified as a parton associated with the wavefunction of the proton. However, the remainder of the pair phase space gives a logarithmically dominant contribution to the leading twist structure functions and can be associated with photon-gluon subprocesses or terms in the logarithmic evolution and hard radiative corrections of the target structure function. In order to keep the analysis as simple as possible, the calculation is presented for the case of spinless quarks. The main effect of spin one-half quarks is simply to reverse the role of σ_L and σ_T in the final formulae.

The kinematics of DIS in the laboratory frame and the connection to light-cone variables are discussed in section 2. In section 3 we analyze the scaling violation of the virtual photo–absorption cross sections. In the simplest version of the model, with scalar quarks, the scalar photo–absorption cross section is logarithmically dominant over the transverse cross section. In order to keep the formulae trans-

parent we will focus on the calculation assuming Coulomb gluon exchange; i.e., a massive source. In order to understand the physics of shadowing and other coherent processes in a nuclear target, it is also important to analyze the transverse separation of the quarks in the pair. This is most easily done by using a Fourier transform in transverse space [9]. The physics of shadowing also requires a detailed understanding of the formation time of the quark pair. As we show in section 4, the Ioffe time can be precisely obtained by differentiating with respect to the relevant energy denominator in time–ordered perturbation theory.

2. Space-Time Kinematics of Deep Inelastic Scattering

As noted in the introduction, the laboratory and Drell-Yan frames give two different physical pictures of DIS. At low x_{bj} the laboratory frame emphasizes the physics from the standpoint of the dissociating virtual photon. At large x_{bj}, the light-cone picture seems more natural, emphasizing the parton structure of the nucleon. In this section we demonstrate the interconnection between these two perspectives of DIS. In the following sections we shall show how the Ioffe time enters into physical processes and where the leading logarithmic contributions to structure functions arise in terms of the kinematics of the pair dissociation process.

The DIS structure functions at $q^2 = -Q^2$, $F_i(x, Q^2)$, are generally identified with the probability distribution $G_{q/p}(x, Q^2)$ for quarks in the nucleon through the leading twist relation Eq. (1.1), where the parameter x_{bj} is identified with $x = \ell^+/p^+$, the light-cone momentum fraction of the struck quark. (We define $p^\pm = p^0 \pm p^z$). This connection can be made explicit in the Drell-Yan frame where

the photon direction is transverse to the proton ($Q^2 = \vec{q}_\perp^{\,2}$)

$$p^\mu = (p^+, p^-, \vec{p}_\perp) = \left(p^+, \frac{M^2}{p^+}, \vec{0}_\perp\right)$$

$$q^\mu = (q^+, q^-, \vec{q}_\perp) = \left(0, \frac{2q\cdot p}{p^+}, \vec{q}_\perp\right) \tag{2.1}$$

$$\ell^\mu = (\ell^+, \ell^-, \vec{\ell}_\perp) = \left(xp^+, \frac{\ell^2 + \ell_\perp^2}{xp^+}, \vec{\ell}_\perp\,.\right)$$

In this frame, the only light-cone time-ordered diagram that needs to be considered is that shown in Fig. 1. Since $q^+ = 0$, pair creation graphs do not occur. In light-cone gauge, $A^+ = 0$, soft final state interactions of the struck quark can be neglected to leading order in $1/Q^2$. QCD evolution equations in $\ell n\, Q^2$ can be derived by taking into account gluonic radiation by the struck quark.

The essential advantage of the Drell-Yan frame is the immediate connection of the DIS process to the parton structure of the proton itself. However, in the high energy domain where $2p\cdot q \gg Q^2$, *i.e.* $x_{bj} \to 0$, it is more natural to think of the DIS process in terms of the structure of the virtual photon, as in Fig. 3. For example, in the laboratory frame where $\vec{q}^{\,2} = \nu^2 + Q^2$ the pair state with invariant mass $\mathcal{M}_{\rm pair}$ is off the energy shell by the amount

$$\Delta E = \sqrt{\mathcal{M}_{\rm pair}^2 + \vec{q}^{\,2}} - \sqrt{q^2 + \vec{q}^{\,2}} \cong \frac{\mathcal{M}_{\rm pair}^2 + Q^2}{2\nu}\,. \tag{2.2}$$

Thus from the perspective of the lab frame, the photon transforms into a virtual quark anti-quark pair at a time

$$\tau = \frac{2\nu}{\mathcal{M}_{\rm pair}^2 + Q^2} \sim \mathcal{O}\left(\frac{1}{M x_{\rm bj}}\right) \tag{2.3}$$

before it interacts with the target, where M is the target mass.

From the covariant point of view, Figs. 1 and 2a are actually different manifestations of the same Feynman diagram (see Fig. 5). We can consider the general frame

$$\begin{aligned} q &= (q^+, q^-, \vec{q}_\perp) = \left(\frac{q^2 + \vec{q}_\perp^{\,2}}{q^-}, q^-, \vec{q}_\perp \right) \\ p &= (p^+, p^-, \vec{p}_\perp) = \left(p^+, \frac{M^2 + \vec{p}_\perp^{\,2}}{p^+}, \vec{p}_\perp \right) \end{aligned} \tag{2.4}$$

where

$$2q \cdot p = 2M\nu = q^+ p^- + q^- p^+ - 2\vec{q}_\perp \cdot \vec{p}_\perp \, . \tag{2.5}$$

If we consider ℓ to be a constituent of the target, then it is natural to parametrize its four-vector in the form

$$\ell^\mu = \left(x p^+, \frac{\ell^2 + (\vec{\ell}_\perp + x\vec{p}_\perp)^2}{x p^+}, \vec{\ell}_\perp + x\vec{p}_\perp \right) \tag{2.6}$$

where $\vec{\ell}_\perp$ is perpendicular to $\vec{p}_\perp$. Similarly, the outgoing quark is naturally considered a fragment of the incoming photon. Thus we parametrize its four-vector as

$$u = \left(\frac{m^2 + (\alpha\vec{q}_\perp + \vec{u}_\perp)^2}{\alpha q^-}, \alpha q^-, \alpha\vec{q}_\perp + \vec{u}_\perp \right) \tag{2.7}$$

where $\vec{u}_\perp$ is perpendicular to $\vec{q}_\perp$ and α is the fraction of the virtual photon momentum carried by the outgoing quark. On the other hand, u^μ is also determined from four-momentum conservation $u^\mu = \ell^\mu + q^\mu$. We thus have the general

relations:

$$xp^+ = \left[\frac{m^2 + \alpha^2 \vec{q}_\perp^{\,2} + \vec{u}_\perp^{\,2}}{\alpha} - (q^2 + \vec{q}_\perp^{\,2})\right] \frac{1}{q^-} ,$$
$$\frac{\ell^2 + \vec{\ell}_\perp^{\,2} + x^2 \vec{p}_\perp^{\,2}}{xp^+} = q^-(\alpha - 1) , \tag{2.8}$$

and

$$\vec{\ell}_\perp + x\,\vec{p}_\perp = (\alpha - 1)\,\vec{q}_\perp + \vec{u}_\perp . \tag{2.9}$$

For example, in any collinear frame with $\vec{q}_\perp = \vec{p}_\perp = 0$, $p^+q^- = 2p \cdot q + Q^2M^2/(p^+q^-) \sim 2p \cdot q$. Then $\vec{\ell}_\perp = \vec{u}_\perp$,

$$x = \frac{Q^2}{2p \cdot q} \left[1 + \frac{m^2 + \vec{u}_\perp^{\,2}}{\alpha Q^2}\right] , \tag{2.10}$$

and

$$\alpha - 1 = \frac{\ell^2 + \vec{\ell}_\perp^{\,2}}{2xp \cdot q} . \tag{2.11}$$

The traditional parton model integration corresponds to limited transverse momenta $u_\perp^2$ or $\ell_\perp^2$, and finite off-shell mass of the struck parton, ℓ^2. Thus $x \Rightarrow x_{bj} = Q^2/2p \cdot q$, and $\alpha \sim 1 - O(1/Q^2)$. In this kinematic regime, the struck quark then takes nearly all of the momentum of the incident photon. The assumption that ℓ^2 is finite can also be understood as a limit on the invariant mass $\mathcal{M}_{spect}$ of the spectator system: $(p - \ell)^2 = \mathcal{M}_{spect}^2$ in Fig. 5. (Again, we take $\vec{p}_\perp = 0$)

$$(p - \ell)^\mu = \left[(1 - x)p^+, \frac{\mathcal{M}_{spect}^2 + \vec{\ell}_\perp^{\,2}}{(1 - x)p^+}, -\vec{\ell}_\perp\right]$$
$$\frac{\ell^2 + \ell_\perp^2}{x} = M^2 - \frac{\mathcal{M}_{spect}^2 + \vec{\ell}_\perp^{\,2}}{1 - x} \tag{2.12}$$

and

$$(1-\alpha) = \frac{1}{2p\cdot q}\,\frac{1}{1-x}\,\left[\ell_\perp^2 + \mathcal{M}_{spect}^2 - (1-x)M^2\right] \ . \tag{2.13}$$

It is then an important question whether one can accurately neglect the kinematic corrections due to $\ell_\perp^2$, $\mathcal{M}_{spect}^2$ since these are variables that are integrated over in the inclusive cross section. The range of these values not only sets the corrections to the $x = x_{bj}$ relation, but also determines the characteristic time and impact separation which dominates the DIS process.

In order to understand the ranges of these kinematic variables, let us look at a typical gauge theory contribution derived from gluon exchange in the t-channel (see Fig. 3). This is essentially Bethe-Heitler pair production in the field of the target. The spin-one gluon in the t-channel leads to an energy-independent contribution to the virtual photon-nucleon cross section in the scaling limit. It is thus a leading contribution to the DIS leading twist structure functions in the small x_{bj} regime. From the standpoint of evolution equations, one encounters this type of contribution after two applications of the QCD splitting functions; thus this contribution appears in the logarithmic evolution of the leading order singlet structure functions. Hence the transverse momentum integrations are logarithmic in nature with a range extending up to $\mathcal{O}(Q^2)$. We thus expect significant numerical corrections to the parton relations:

$$\begin{aligned}
x &= x_{bj}\left[1 + \frac{m^2 + u_\perp^2}{\alpha Q^2}\right] = x_{bj}\left[1 + \frac{\mathcal{O}(1)}{\log Q^2}\right] \\
\tau &= \frac{2\nu}{\mathcal{M}_{\rm pair}^2 + Q^2} = \left(\frac{1}{M x_{bj}}\right)\left[1 + \frac{\mathcal{O}(1)}{\log Q^2}\right] \\
1-\alpha &= \frac{1}{2p\cdot q}\,\frac{1}{1-x}\,\left[\ell_\perp^2 + \mathcal{M}_{spect}^2 - (1-x)M^2\right] \ .
\end{aligned} \tag{2.14}$$

Note that the deviation of x from x_{bj} affects the accuracy of sum rules, etc. based on parton model distributions.

It should be noted that it is only the strictly asymmetric region where one quark carries all of the energy ν of the photon and the other quark has finite momentum in the target rest frame that corresponds to the traditional parton model. In this case the intermediate quark line can be considered as a constituent of the target. For example in Fig. 3 let us assume that u is finite; then w carries all the energy ν of the photon, and also has limited transverse momentum $w_\perp \simeq -u_\perp$. Since $(u+k)^2$ is finite and

$$q^2 = (u+k+w)^2 \simeq (u+k)^2 + 2\nu(u^o + k^o - u^z - k^z),$$

we have

$$(u^o + k^o - u^z - k^z)/M = -Q^2/(2M\nu) = -x$$

which gives the connection between the Bjorken variable and the light-cone momentum fraction of the quark constituent of the target with momentum $-(u+k)$. On the other hand, if the gluon had attached itself to the energetic quark w, then the virtuality of that quark line before the gluon vertex would be large:

$$(w+k)^2 = 2\nu(k^o - k^z) = O(\nu)$$

which suppresses this diagram compared to the interaction with the slow quark u. When one integrates over the full phase space of the Bethe-Heitler process, one finds that the strictly asymmetric region is just the endpoint of a logarithmic integration region, providing leading–twist contributions to the structure functions beyond

what is contained in the traditional parton model. The leading–twist contributions from the pair production processes with symmetric kinematics may be associated with the photon – gluon fusion subprocess $\gamma^* + g \to q\bar{q}$. In the symmetric region one sees explicitly the effect of charge (or color) screening: up to logarithmic corrections, the cross section scales as $1/Q^2$, because of the destructive interference between the quark and anti-quark scattering amplitudes.

3. Bethe-Heitler pair production

In order to understand the relationship of Bethe-Heitler pair production to deep inelastic lepton scattering, we will consider the simplest model which demonstrates the essential features, namely scalar charged particle production in QED with a fixed coupling constant. Since we wish to understand the role of the Ioffe time, we work in time-ordered perturbation theory. One can show that the lepton interaction can be replaced by an incident photon with effective spacelike mass q^2, just as in conventional covariant perturbation theory [11] . Again for simplicity, we consider scattering on a target of large mass M. In the large target-mass limit, we may approximate the photon k^μ exchanged between the pair and the target with a Coulomb photon and take $k^0 = -k^2/2M \simeq 0$. Because of the Coulomb interaction, the seagull diagrams do not contribute in Coulomb gauge. The surviving four time-ordered diagrams are given in Fig. 6, where the kinematic notation is also introduced. Using gauge invariance with respect to the virtual photon current, the amplitudes in the lab frame for scalar and transverse photons are, respectively,

$$M_S = (-ie)^3 \sqrt{\frac{Q^2}{\nu^2+Q^2}}\,\frac{M}{\vec{k}^2} \left[\frac{(E_{u'}-E_w)(E_u+E_{u'})}{E_{u'}(E_u-E_{u'})} + \frac{(E_u-E_{u'})(E_w+E_{u'})}{E_{u'}(E_u+E_{u'})} + (\vec{u}\leftrightarrow\vec{w})\right], \tag{3.1}$$

$$M_T = (-ie)^3\,\frac{2M}{\vec{k}^2}\left[\left(\frac{E_u+E_{u'}}{E_{u'}(E_u-E_{u'})} - \frac{E_u-E_{u'}}{E_{u'}(E_u+E_{u'})}\right)\vec{w}\cdot\vec{\epsilon}_T(\vec{q}) + (\vec{u}\leftrightarrow\vec{w})\right], \tag{3.2}$$

with $E_{u'} = [E_u^2 + (2\vec{u}+\vec{k})\cdot\vec{k}]^{1/2}$. (The diagrams where the Coulomb photon is exchanged between the target and the charged scalar $\vec{w}$ are obtained from the ones written explicitly by exchanging $\vec{u}$ and $\vec{w}$.) The contribution of the backward-propagating diagrams in Eq. (3.1), (3.2) is $O(Q^2/\nu^2)$ with respect to the contribution of the forward-propagating ones.

After some algebra and summing over the photon polarization, the scalar and transverse photo-absorption cross sections can be written in a compact form:

$$\sigma_S = \frac{\alpha_{em}^3}{\pi^2}Q^2\int_0^1 d\alpha(2\alpha-1)^2\alpha(1-\alpha)\int d^2\vec{u}_\perp\int d^2\vec{k}_\perp\frac{1}{(\vec{k}^2)^2} \left(\frac{1}{\vec{u}_\perp^2+\beta^2} - \frac{1}{(\vec{u}_\perp+\vec{k}_\perp)^2+\beta^2}\right)^2, \tag{3.3}$$

$$\sigma_T = \frac{4\alpha_{em}^3}{\pi^2}\int_0^1 d\alpha\alpha(1-\alpha)\int d^2\vec{u}_\perp\int d^2\vec{k}_\perp\frac{1}{(\vec{k}^2)^2} \left[\frac{\vec{u}_\perp^2}{(\vec{u}_\perp^2+\beta^2)^2} + \frac{(\vec{u}_\perp+\vec{k}_\perp)^2}{[(\vec{u}_\perp+\vec{k}_\perp)^2+\beta^2]^2} - \frac{2\vec{u}_\perp\cdot(\vec{u}_\perp+\vec{k}_\perp)}{(\vec{u}_\perp^2+\beta^2)[(\vec{u}_\perp+\vec{k}_\perp)^2+\beta^2]}\right], \tag{3.4}$$

with

$$\vec{k}^2 = \vec{k}_\perp^2 + k_z^2,$$
$$\beta^2 = m^2 + \alpha(1-\alpha)Q^2,$$

where m and α are respectively the mass and the fractional energy of the scalar particles. As we are in the large target mass M limit, the energies of the produced scalars add up to the energy of the virtual photon. Higher twist corrections of order Q^2/ν^2 to the cross sections are neglected.

In Eqs. (3.3), (3.4) we expanded in $\vec{u}_\perp^2/E_u^2$ and $\vec{w}_\perp^2/E_w^2$, assuming that the transverse components of the pair are much smaller than the respective longitudinal ones. The regions of phase space where this is not true can be neglected, since in such regions the longitudinal and/or transverse momentum components of the exchanged photon are large, and the Coulomb propagator acts as an effective cutoff. We have checked numerically that the difference between the exact expressions for the cross sections, from Eq. (3.1) and (3.2), and their approximations (3.3), (3.4) is less than 10%, at the typical kinematics of the EMC experiment; i.e., $Q^2 = 19$ GeV^2 and $\nu = 113$ GeV [12] .

From momentum conservation and the expansion in the transverse momentum of the pair, the longitudinal momentum of the Coulomb photon is

$$k_z \simeq x_{bj}M + \mu^2/2\nu, \tag{3.5}$$

where $\mu^2 \simeq (\vec{u}_\perp^2 + m^2)/\alpha(1-\alpha)$ is the invariant mass of the produced pair. Since the main contribution to the cross sections comes from pairs of mass $\mu^2 \approx Q^2$ [10], in the following analytic calculations we take k_z constant[2].

2 In a numeric analysis though, in which one uses the exact expressions (3.1) and (3.2) and integrates over the whole phase space, it is important to keep $k_z = \nu + x_{bj}M - u_z - w_z$ as given in general by momentum conservation. In those phase space regions where the approximate formulae (3.3) and (3.4) fail, k_z is large and suppresses the cross sections. This is true even when the Coulomb photon is given an effective mass.

We introduce the impact parameter $\vec{\rho}$ representation and its Fourier transforms [9,10]

$$\int \frac{d^2\vec{u}_\perp}{(\vec{u}_\perp^2+\beta^2)[(\vec{u}_\perp+\vec{k}_\perp)^2+\beta^2]} = \int d^2\vec{\rho} e^{i\vec{\rho}\cdot\vec{k}_\perp} \left| \frac{1}{2\pi} \int d^2\vec{u}_\perp \frac{e^{i\vec{\rho}\cdot\vec{u}_\perp}}{\vec{u}_\perp^2+\beta^2} \right|^2, \tag{3.6}$$

$$\begin{aligned} &\int d^2\vec{u}_\perp \frac{\vec{u}_\perp\cdot(\vec{u}_\perp+\vec{k}_\perp)}{(\vec{u}_\perp^2+\beta^2)[(\vec{u}_\perp+\vec{k}_\perp)^2+\beta^2]} = \\ &\frac{1}{(2\pi)^2} \int d^2\vec{\rho} e^{i\vec{\rho}\cdot\vec{k}_\perp} \int d^2\vec{u}_{1\perp} d^2\vec{u}_{2\perp} \frac{\nabla_\rho e^{i\vec{\rho}\cdot\vec{u}_{1\perp}} \cdot \nabla_\rho e^{-i\vec{\rho}\cdot\vec{u}_{2\perp}}}{(\vec{u}_{1\perp}^2+\beta^2)(\vec{u}_{2\perp}^2+\beta^2)}, \end{aligned} \tag{3.7}$$

in Eq. (3.3), (3.4). After doing all the angular integrations, and the one over the transverse size of the pair by using the relationship [13]

$$\int_0^\infty dx \frac{x^{\nu+1} J_\nu(\rho x)}{(x^2+\beta^2)^{\mu+1}} = \frac{\beta^{\nu-\mu}\rho^\mu}{2^\mu \Gamma(\mu+1)} K_{\nu-\mu}(\rho\beta), \tag{3.8}$$

the photo–absorption cross sections σ_S and σ_T become

$$\sigma_S = 4\alpha_{em}^3 Q^2 \int_0^1 d\alpha (2\alpha-1)^2 \alpha(1-\alpha) \int dk_\perp^2 \frac{1}{(\vec{k}^2)^2} \int d\rho\rho \left[1 - J_0(\rho k_\perp)\right] K_0(\rho\beta)^2, \tag{3.9}$$

$$\sigma_T = 16\alpha_{em}^3 \int_0^1 d\alpha \alpha(1-\alpha)\beta^2 \int dk_\perp^2 \frac{1}{(\vec{k}^2)^2} \int d\rho\rho \left[1 - J_0(\rho k_\perp)\right] K_1(\rho\beta)^2. \tag{3.10}$$

An analysis of (3.9) and (3.10) shows that terms proportional to the quark mass m give only higher twist corrections; since the pair mass μ is large, there are no logarithmic mass divergences. As we limit our analysis to the leading twist contributions, we can neglect m in the following.

We will perform the integral over the impact parameter ρ first since this is advantageous for the computation of the Ioffe time. The impact integral can be done through the relationship [13]

$$\int d\rho\rho\big[1 - J_0(\rho k_\perp)\big] K_\nu(\rho\beta)^2 = \\ \frac{1}{2\beta^2}\Gamma(1+\nu)\Gamma(1-\nu)\Big[1 - \Big(\frac{u+1}{2}\Big)^{\nu-1} F\Big(\frac{1}{2} - \nu; 1-\nu; \frac{3}{2}; \frac{u-1}{u+1}\Big)\Big], \tag{3.11}$$

where $u = 1 + k_\perp^2/2\beta^2$. The study of Eq. (3.11) is done in the appendix, where we consider 2 kinematic regions (Fig. 7)

$$i)\ k_\perp^2 \leq 4\beta^2 \tag{3.12}$$

$$ii)\ k_\perp^2 > 4\beta^2. \tag{3.13}$$

The parton model contribution where σ_S satisfies Bjorken scaling and σ_T is higher twist comes from the endpoint of region $ii)$ with α or $(1-\alpha) < k_\perp^2/4Q^2$ and $k_\perp^2$ constant and much smaller than Q^2.

In the kinematic region $i)$, which will be the logarithmically dominant region, α takes the values

$$1 - \sqrt{1 - \frac{k_\perp^2}{Q^2}} \leq 2\alpha \leq 1 + \sqrt{1 - \frac{k_\perp^2}{Q^2}}. \tag{3.14}$$

After integrating over ρ (see appendix), we find that in the region $i)$

$$\sigma_S = \frac{1}{3}\frac{\alpha_{em}^3}{Q^2}\int dk_\perp^2 \frac{k_\perp^2}{(\vec{k}^2)^2}\int d\alpha \frac{(2\alpha-1)^2}{\alpha(1-\alpha)}, \tag{3.15}$$

$$\sigma_T = \frac{8}{3}\frac{\alpha_{em}^3}{Q^2}\int dk_\perp^2 \frac{k_\perp^2}{(\vec{k}^2)^2}\int d\alpha. \tag{3.16}$$

In (3.15) both the integrations over α and $k_\perp^2 > k_z^2$ contribute a logarithmic en-

hancement [10], whereas in (3.16) the integration over α is regular. In both cases the integration over $k_\perp^2 < k_z^2$ is logarithmically suppressed since the longitudinal momentum of the Coulomb photon acts as a cutoff. The leading behavior of Eq. (3.15) and (3.16) is given in Table 1. The logarithmic enhancement in σ_S from the endpoint integration over α corresponds to the dominance of the asymmetric pair region. As expected, we get logarithmic scaling violations to the scaling predicted by the parton model for the photo–absorption cross sections.

Table 1: Leading log behavior

of the photo–absorption cross sections

Scalar QED	$k_\perp^2 \leq 4\beta^2$	$k_\perp^2 > 4\beta^2$
$Q^2\sigma_S$	$\ell n^2(Q^2/k_z^2)$	$\ell n(Q^2/k_z^2)$
$Q^2\sigma_T$	$\ell n(Q^2/k_z^2)$	const

After the integration on the impact parameter (see appendix), we obtain in the region *ii*)

$$\sigma_S = 2\alpha_{em}^3 \int dk_\perp^2 \frac{1}{(\vec{k}^2)^2} \int d\alpha (2\alpha - 1)^2, \tag{3.17}$$

$$\sigma_T = 8\alpha_{em}^3 \int dk_\perp^2 \frac{1}{(\vec{k}^2)^2} \int d\alpha \alpha(1-\alpha) \Big(\ell n \frac{k_\perp^2}{4\beta^2} + \frac{1}{3} \Big). \tag{3.18}$$

In (3.17) and (3.18) the integration over α, in the range complementary to (3.14), is regular. The integration over $k_z^2 < k_\perp^2 < Q^2$ gives a logarithmic contribution in the scalar case, whereas it is regular in the transverse case. The integration over $k_\perp^2 < k_z^2$ is again suppressed, so that in this region (3.17) satisfies Bjorken scaling and (3.18) is higher twist. Finally, the region of integration with $Q^2 < k_\perp^2 < \nu^2$

corresponds to hard radiative corrections, and has no logarithmic enhancements, so that (3.17) and (3.18) satisfy Bjorken scaling in this region.

Thus the complete leading log contribution from Bethe-Heitler pair production to deep inelastic lepton scattering cross sections is contained in the full region i), whereas the contribution of region ii) is next-to-leading, both in the scalar and transverse photon case (Table 1).

A numerical check of the scaling violation, at fixed x_{bj}, of the exact massless cross sections, through Eq. (3.1) and (3.2), vs. the leading-log scaling violations from Table 1 is given in in Fig. 8, where, for sake of comparison, we take $k_z \simeq 2x_{bj}M$ according to the previous considerations on the longitudinal size of the Coulomb photon. The agreement for the scalar cross section is excellent; in the transverse case, next-to-leading (constant) corrections appear to be significant.

The ratio of the scalar to the transverse cross sections,

$$\frac{\sigma_S}{\sigma_T} \propto \ell n \frac{Q^2}{k_z^2}, \tag{3.19}$$

diverges for large ν and fixed x_{bj}. This is the expected logarithmic correction to the Callan-Gross relation for scalar quark QED. The leading–log violations to the structure functions

$$4\pi^2 \alpha_{em} F_2(x_{bj}) = Q^2(\sigma_S + \sigma_T)$$

$$4\pi^2 \alpha_{em} 2x_{bj} F_1(x_{bj}) = Q^2 \sigma_T$$

can also be obtained from Table 1.

We identify the transverse size of the pair, as a function of the longitudinal momentum of the quark, with the mean separation in impact parameter space:

$$\langle \rho_i^2(\alpha) \rangle = \frac{1}{d\sigma_i/d\alpha} \int dk_\perp^2 d\rho \rho^2 \frac{d^3\sigma_i}{dk_\perp^2 d\rho d\alpha}, \tag{3.20}$$

where $i = S, T$ and $d\sigma_i/d\alpha$ for Bethe-Heitler pairs is obtained from Eqs. (3.15), (3.17) and (3.16), (3.18). To compute Eq. (3.20) we take $d^3\sigma_i/dk_\perp^2 d\rho d\alpha$ from Eqs. (3.9) and (3.10) and consider the different asymptotic expansions of the Bessel function J; namely $i)$ $\rho k_\perp \leq 2$ and $ii)$ $\rho k_\perp > 2$. Because of the asymptotic convergence of the Bessel function K, in either region the main contribution to the integration over ρ in Eq. (3.20) comes from $\rho \simeq \beta^{-1}$, thus regions $i)$ and $ii)$ coincide with regions (3.12) and (3.13). We define $I(n,\nu)$ as the corresponding integral over the impact parameter and we compute it through the relationship [13]

$$I(n,\nu) \equiv \int_0^\infty dx x^n K_\nu(x)^2 = \frac{2^{n-2}}{\Gamma(1+n)} \Gamma\Big(\frac{1+n+2\nu}{2}\Big) \Gamma\Big(\frac{1+n}{2}\Big)^2 \Gamma\Big(\frac{1+n-2\nu}{2}\Big). \tag{3.21}$$

Summing the contribution of regions (3.12) and (3.13) to Eq. (3.20), we obtain

$$\langle \rho_S^2(\alpha) \rangle = \frac{1}{\alpha(1-\alpha)Q^2} \frac{I(5,0) f(\alpha) + 4I(3,0) g(\alpha)}{I(3,0) f(\alpha) + 4I(1,0) g(\alpha)} \tag{3.22}$$

$$\langle \rho_T^2(\alpha) \rangle = \frac{1}{\alpha(1-\alpha)Q^2} \frac{I(5,1) f(\alpha) + 4I(3,1) g(\alpha)}{I(3,1)\big(f(\alpha)+g(\alpha)\big) + 2\frac{Q^2}{k_z^2} \ell n\big(1 + \frac{k_z^2}{4\alpha(1-\alpha)Q^2}\big)}, \tag{3.23}$$

where

$$f(\alpha) = \frac{1}{\alpha(1-\alpha)} \ell n\Big(1 + 4\alpha(1-\alpha)\frac{Q^2}{k_z^2}\Big); \; g(\alpha) = \frac{Q^2/k_z^2}{1 + 4\alpha(1-\alpha)Q^2/k_z^2}. \tag{3.24}$$

Taking the soft quark limit ($\alpha < k_z^2/4Q^2$), we find

$$\lim_{\alpha\to 0,1}\left\langle \rho_S^2(\alpha)\right\rangle = \frac{I(5,0)+I(3,0)}{I(3,0)+I(1,0)}\frac{1}{\alpha(1-\alpha)Q^2} = \frac{42}{25}\frac{1}{\alpha(1-\alpha)Q^2}, \tag{3.25}$$

$$\begin{aligned}\lim_{\alpha\to 0,1}\left\langle \rho_T^2(\alpha)\right\rangle =& 2[I(5,1)+I(3,1)]\frac{1}{\alpha(1-\alpha)Q^2\ell n[k_z^2/4\alpha(1-\alpha)Q^2]} \\ =& \frac{68}{15}\frac{1}{\alpha(1-\alpha)Q^2\ell n[k_z^2/4\alpha(1-\alpha)Q^2]}.\end{aligned} \tag{3.26}$$

Thus the transverse size of the pair grows as the longitudinal momentum of the quark becomes small. The fact that the impact separation is larger for scalar photons compared to transverse photons is consistent with the larger scalar cross section for spinless partons.

4. Ioffe time

According to the definition given in the introduction, the Ioffe time τ is the distance between the point of interaction of the Bethe-Heitler pair with the virtual photon and the point of interaction with the Coulomb photon. Thus, using Eqs. (2.3) and (3.5), we find, by the uncertainty relation, that the Ioffe time is approximately given by the inverse of the longitudinal momentum (3.5) of the Coulomb photon[3], and depends on the invariant mass μ of the pair.

In this section we estimate the Ioffe time averaging the contribution of the scattering amplitudes at fixed τ. As we see from Fig. 6, τ is positive for forward-propagating diagrams and negative for the backward-propagating ones. Using

[3] In time-ordered perturbation theory and in the large target-mass limit, the invariant mass of the pair is the same, before ($\mathcal{M}^2_{\rm pair}$) and after (μ^2) the emission of the Coulomb photon, up to corrections of higher order.

time–ordered perturbation theory, the photo–absorption amplitudes at fixed τ in the target frame are

$$\begin{aligned}\frac{dM_S(\tau)}{d\tau} =& e^3\sqrt{\frac{Q^2}{\nu^2+Q^2}}\frac{M}{\vec{k}^2}\Big[e^{i\tau(E_u-E_{u'})}\frac{(E_{u'}-E_w)(E_u+E_{u'})}{E_{u'}}\theta(\tau)\\ &- e^{i\tau(E_u+E_{u'})}\frac{(E_u-E_{u'})(E_w+E_{u'})}{E_{u'}}\theta(-\tau)+(\vec{u}\leftrightarrow\vec{w})\Big],\end{aligned} \tag{4.1}$$

$$\begin{aligned}\frac{dM_T(\tau)}{d\tau} =& e^3\frac{2M}{\vec{k}^2}\Big[\Big(e^{i\tau(E_u-E_{u'})}\frac{E_u+E_{u'}}{E_{u'}}\theta(\tau)\\ &+ e^{i\tau(E_u+E_{u'})}\frac{E_u-E_{u'}}{E_{u'}}\theta(-\tau)\Big)\vec{w}\cdot\vec{\epsilon}_T(\vec{q})+(\vec{u}\leftrightarrow\vec{w})\Big].\end{aligned} \tag{4.2}$$

Integrating (4.1) and (4.2) over τ we recover the photo–absorption amplitudes of Eq. (3.1) and (3.2). It is easy to see from the expansion of the arguments of the exponentials that the backward-propagating diagrams are short range in τ, while the forward-propagating ones, which give the leading twist contributions, are long–range and the corresponding time τ scales like $(x_{bj}M)^{-1}$.

Let us identify the mean Ioffe time through the statistical average

$$\langle\tau\rangle_i^2=\frac{1}{\sigma_i}\int d(PS)\sum_{pol}\left|\int d\tau\tau\frac{dM_i(\tau)}{d\tau}\right|^2,\quad i=S,T \tag{4.3}$$

where the photo–absorption cross sections are

$$\sigma_i=\int d(PS)\sum_{pol}\left|\int d\tau\frac{dM_i(\tau)}{d\tau}\right|^2,\quad i=S,T \tag{4.4}$$

where the sum is over photon polarization.

We now follow the outline ofsection 2; namely, we compute the exact expression for $\int d\tau \tau dM_i(\tau)/d\tau$ (which we will also use for numerical calculations), expand it in the transverse momenta of the pair in order to derive a simple analytical expression for $\langle\tau\rangle_i^2$, and go to the impact parameter representation. The required integrals are:

$$\int_{-\infty}^{\infty} d\tau \tau \frac{dM_S(\tau)}{d\tau} = -e^3 \sqrt{\frac{Q^2}{\nu^2+Q^2}} \frac{M}{\vec{k}^2} \left[\frac{(E_{u'}-E_w)(E_u+E_{u'})}{E_{u'}(E_u-E_{u'})^2} + \frac{(E_u-E_{u'})(E_w+E_{u'})}{E_{u'}(E_u+E_{u'})^2} + (\vec{u} \leftrightarrow \vec{w}) \right], \tag{4.5}$$

$$\int_{-\infty}^{\infty} d\tau \tau \frac{dM_T(\tau)}{d\tau} = -e^3 \frac{2M}{\vec{k}^2} \left[\left(\frac{E_u+E_{u'}}{E_{u'}(E_u-E_{u'})^2} - \frac{E_u-E_{u'}}{E_{u'}(E_u+E_{u'})^2} \right) \vec{w} \cdot \vec{\epsilon}_T(\vec{q}) + (\vec{u} \leftrightarrow \vec{w}) \right], \tag{4.6}$$

As in Eqs. (3.3) and (3.4), we expand in transverse momentum. Then using Eq. (4.3), the mean square Ioffe time for scalar and transverse photons is

$$\langle\tau\rangle_S^2 = \frac{1}{\sigma_S} \frac{4\alpha_{em}^3}{\pi^2} Q^2 \nu^2 \int_0^1 d\alpha (2\alpha-1)^2 \alpha^3 (1-\alpha)^3 \int d^2k \frac{1}{(\vec{k}^2)^2} \int d^2u \left(\frac{1}{(\vec{u}_\perp^2+\beta^2)^2} - \frac{1}{[(\vec{u}_\perp+\vec{k}_\perp)^2+\beta^2]^2} \right)^2, \tag{4.7}$$

$$\langle\tau\rangle_T^2 = \frac{1}{\sigma_T}\frac{16\alpha_{em}^3}{\pi^2}\nu^2 \int_0^1 d\alpha\alpha^3(1-\alpha)^3 \int d^2k \frac{1}{(\vec{k}^2)^2} \int d^2u$$
$$\left[\frac{\vec{u}_\perp^2}{(\vec{u}_\perp^2+\beta^2)^4} + \frac{(\vec{u}_\perp+\vec{k}_\perp)^2}{[(\vec{u}_\perp+\vec{k}_\perp)^2+\beta^2]^4} - \frac{2\vec{u}_\perp\cdot(\vec{u}_\perp+\vec{k}_\perp)}{(\vec{u}_\perp^2+\beta^2)^2[(\vec{u}_\perp+\vec{k}_\perp)^2+\beta^2]^2}\right], \tag{4.8}$$

up to higher–twist terms of $O(Q^2/\nu^2)$. By Fourier-transforming in ρ and integrating over the angular variables and the transverse momentum $u_\perp$ of the pair using Eq. (3.8), we can express the Ioffe time in terms of Bessel functions of the impact parameter

$$\langle\tau\rangle_S^2 = \frac{1}{\sigma_S}4\alpha_{em}^3 Q^2\nu^2 \int_0^1 d\alpha \frac{(2\alpha-1)^2\alpha^3(1-\alpha)^3}{\beta^2} \int dk_\perp^2 \frac{1}{(\vec{k}^2)^2}$$
$$\int d\rho\rho^3\left[1-J_0(\rho k_\perp)\right]K_1(\rho\beta)^2, \tag{4.9}$$

$$\langle\tau\rangle_T^2 = \frac{1}{\sigma_T}16\alpha_{em}^3\nu^2 \int_0^1 d\alpha\alpha^3(1-\alpha)^3 \int dk_\perp^2 \frac{1}{(\vec{k}^2)^2}$$
$$\int d\rho\rho^3\left[1-J_0(\rho k_\perp)\right]K_0(\rho\beta)^2. \tag{4.10}$$

The asymptotic analysis of Eqs. (4.9) and (4.10), through the asymptotic expansions of the Bessel functions, shows that the leading logarithmic contribution comes from region i), Eq. (3.12), as in the case of the photo–absorption cross sections. Mass terms can again be neglected since they only yield higher twist corrections.

In region i), after integrating over ρ, by using Eq. (3.21), the leading logarithmic contribution to the mean–square Ioffe time is

$$\langle\tau\rangle_S^2 = \frac{1}{\sigma_S} I(5,1)\alpha_{em}^3 \frac{\nu^2}{Q^6} \int dk_\perp^2 \frac{k_\perp^2}{(\vec{k}^2)^2} \int d\alpha \frac{(2\alpha-1)^2}{\alpha(1-\alpha)}, \tag{4.11}$$

$$\langle\tau\rangle_T^2 = \frac{1}{\sigma_T} 4I(5,0)\alpha_{em}^3 \frac{\nu^2}{Q^6} \int dk_\perp^2 \frac{k_\perp^2}{(\vec{k}^2)^2} \int d\alpha, \tag{4.12}$$

Dividing Eq. (4.11) by (3.15), and Eq. (4.12) by (3.16), and using Eq. (3.21), we find that in the leading logarithmic approximation, the mean–square Ioffe time for scalar and transverse photons respectively is

$$\langle\tau\rangle_S^2 = \frac{6}{5} \frac{1}{(x_{bj}M)^2}, \tag{4.13}$$

$$\langle\tau\rangle_T^2 = \frac{2}{5} \frac{1}{(x_{bj}M)^2}. \tag{4.14}$$

In Fig. 9 we compare the Ioffe time for $m = 0$ obtained from the numerical integration of Eq. (4.3) and the complete amplitudes (4.5) and (4.6), with the leading logarithmic estimate of Eq. (4.13) and (4.14). In either case we find that the agreement between the exact Ioffe time and its logarithmic estimate is good.

We identify the mean Ioffe time, as a function of the longitudinal momentum of the quark, through the statistical average

$$\langle\tau(\alpha)\rangle_i^2 = \frac{1}{d\sigma_i/d\alpha} \int d(PS) \Big|_\alpha \sum_{pol} \left| \int d\tau\tau \frac{dM_i(\tau)}{d\tau} \right|^2, \quad i = S,T \tag{4.15}$$

where integrations in the phase space are done at fixed α. The differential cross section $d\sigma_i/d\alpha$ is defined as in Eq. (4.4) and is obtained for Bethe-Heitler pairs

from Eqs. (3.9) and (3.10). Analysing the behavior of Eq. (4.15) in the regions (3.12) and (3.13), using Eqs. (4.9) and (4.10), the integral (3.21) on the impact parameter, and the functions (3.24), we obtain (Fig. 10)

$$\langle\tau(\alpha)\rangle_S^2 = \frac{\nu^2}{Q^4}\frac{I(5,1)f(\alpha)+4I(3,1)g(\alpha)}{I(3,0)f(\alpha)+4I(1,0)g(\alpha)}, \tag{4.16}$$

$$\langle\tau(\alpha)\rangle_T^2 = \frac{\nu^2}{Q^4}\frac{I(5,0)f(\alpha)+4I(3,0)g(\alpha)}{I(3,1)\big(f(\alpha)+g(\alpha)\big)+2\frac{Q^2}{k_z^2}\ell n\big(1+\frac{k_z^2}{4\alpha(1-\alpha)Q^2}\big)}, \tag{4.17}$$

Taking the soft quark limit ($\alpha < k_z^2/4Q^2$), we find

$$\lim_{\alpha\to 0,1}\langle\tau(\alpha)\rangle_S^2 = \frac{1}{4}\frac{I(5,1)+I(3,1)}{I(3,0)+I(1,0)}\frac{1}{(x_{bj}M)^2} = \frac{17}{25}\frac{1}{(x_{bj}M)^2}, \tag{4.18}$$

$$\begin{aligned}\lim_{\alpha\to 0,1}\langle\tau(\alpha)\rangle_T^2 =& \frac{I(5,0)+I(3,0)}{2}\frac{1}{(x_{bj}M)^2\ell n[k_z^2/4\alpha(1-\alpha)Q^2]}\\ =& \frac{7}{10}\frac{1}{(x_{bj}M)^2\ell n[k_z^2/4\alpha(1-\alpha)Q^2]}.\end{aligned} \tag{4.19}$$

Thus in the scalar case the Ioffe time becomes independent of α in the soft quark limit, in agreement with the parton-model-inspired kinematic relations of Eq. (2.14). In the transverse case, due to the logarithmic corrections, the Ioffe time vanishes in the soft quark limit. This shows that in the parton-model region the space-time behavior of the cross section dramatically depends on the virtual photon polarization, since long-range contributions appear only for the photon polarization corresponding to the leading photo-absorption cross section.

5. Conclusions

As we have discussed in this paper, it is important to understand deep inelastic lepton scattering in the rest frame of the target. In particular, the physics of the small x_{bj} regime is strongly related to pair production in the field of the target. The effect of the nuclear environment is also most easily understood from the perspective of the laboratory frame where the time evolution of the propagating quarks can be analyzed.

The general connection between the kinematics of deep inelastic scattering in the infinite momentum frame and the target rest frame has been presented in section 2. In the general case, one has to allow for logarithmic corrections to the conventional parton model relations, as expressed through Eqs. (2.14).

In section 3, we study the spacetime development of quark pair production, a process which is closely related to the perturbative development of the strange and charm quark sea at low x_{bj}. In this calculation, one can identify the kinematic domain of the traditional Bjorken-scaling parton model as the highly asymmetric region where the longitudinal momentum fraction α of the interacting quark is smaller than $k_\perp^2/4Q^2$ and the transverse momentum $k_\perp^2$ of the exchanged gluon is constant and much smaller than Q^2. The integration over the full kinematics of the pair production process reproduces the logarithmic corrections to the virtual photo-absorption cross sections usually associated with the evolution of the singlet structure functions.

The transverse size of the quark pair can be identified with the average impact parameter ρ. In particular, we show that the transverse size of the pair grows as the longitudinal momentum fraction α of the quark decreases. In the case of spin-less quarks the virtual photo-absorption cross section for scalar photons logarithmically

dominates the cross section for photons with transverse polarization. Similarly, we also find that the transverse size of the quark pair is logarithmically larger in the scalar polarization case, in agreement with geometric considerations.

The Ioffe time τ_I, which gives the coherence length of the pair production process in the target rest frame, can also be computed explicitly in the pair production model. As discussed in section 4, the Ioffe time is approximately equal to the inverse of the longitudinal momentum transfer of the exchanged gluon; its magnitude also reflects the size of the invariant mass of the pair. In general, τ_I is proportional to $1/x_{bj}$. Remarkably, as we show in section 4, the constant of proportionality depends on the virtual photon polarization; e.g., in the case of spinless quarks $\tau_S/\tau_T = \sqrt{3}$, averaging over all kinematic variables. In the parton model region, where α is small, $\tau_T \to 0$ corresponding to zero longitudinal coherence whereas $\tau_s x_{bj} M$ is finite, reflecting the fact that there are long-range contributions to the scalar cross section only.

As noted in the introduction, the ability to control the Ioffe time by changing x_{bj} or the photon polarization allows one to use the nucleus as an instrument to probe quark–nucleon interactions. It is clearly important to study shadowing and anti-shadowing and nuclear modifications of jet hadronization, energy loss, and transverse smearing as a function of photon polarization as well as x_{bj}.

ACKNOWLEDGEMENTS

We thank Lance Dixon and Adam Falk for useful discussions.

APPENDIX

Calculation of $\int d\rho\rho\big[1 - J_0(\rho k_\perp)\big] K_\nu(\rho\beta)^2$.

In the scalar virtual photon case, $\nu = 0$ in Eq. (3.11). Thus

$$\int d\rho\rho\big[1 - J_0(\rho k_\perp)\big] K_0(\rho\beta)^2 = \frac{1}{2\beta^2}\left[1 - \frac{1}{1+\frac{k_\perp^2}{4\beta^2}} F\Big(\frac{1}{2}; 1; \frac{3}{2}; \frac{\frac{k_\perp^2}{4\beta^2}}{1+\frac{k_\perp^2}{4\beta^2}}\Big)\right]$$

$$= \frac{1}{2\beta^2}\left[1 - \frac{1}{\frac{k_\perp}{\beta}\sqrt{1+\frac{k_\perp^2}{4\beta^2}}} \ell n\left(\frac{1+\frac{k_\perp/2\beta}{\sqrt{1+k_\perp^2/4\beta^2}}}{1-\frac{k_\perp/2\beta}{\sqrt{1+k_\perp^2/4\beta^2}}}\right)\right]. \tag{A.1}$$

The expansions of Eq. (A.1) in the 2 kinematic regions *i*) $k_\perp^2 \leq 4\beta^2$ and *ii*) $k_\perp^2 > 4\beta^2$ are

$$i);\ \int d\rho\rho\big[1 - J_0(\rho k_\perp)\big] K_0(\rho\beta)^2 = \frac{1}{3\beta^2}\frac{k_\perp^2}{4\beta^2} + O\Big(\big(\frac{k_\perp^2}{4\beta^2}\big)^2\Big), \tag{A.2}$$

$$ii);\ \int d\rho\rho\big[1 - J_0(\rho k_\perp)\big] K_0(\rho\beta)^2 = \frac{1}{2\beta^2} + O\Big(\frac{4\beta^2}{k_\perp^2}\Big). \tag{A.3}$$

In the transverse virtual photon case, $\nu = 1$ in Eq. (3.11). This, as such, is ill-defined, as one of its Γ functions is singular. The singularity, though, cancels between the 2 terms of the integrand. Thus to extract the finite residue we set $\nu = 1 - \epsilon$ and take the limit for ϵ that goes to 0 at the end. Using the expansion

$$\Gamma(\epsilon) = \frac{1}{\epsilon} - \gamma + O(\epsilon)$$

where γ is the Euler-Mascheroni constant, we obtain

$$\lim_{\epsilon\to 0}\int d\rho\rho\big[1 - J_0(\rho k_\perp)\big] K_{1-\epsilon}(\rho\beta)^2 = \frac{1}{2\beta^2}\Big[\ell n\Big(1+\frac{k_\perp^2}{4\beta^2}\Big) + \frac{1}{3}\frac{k_\perp^2/4\beta^2}{1+k_\perp^2/4\beta^2}\Big]. \tag{A.4}$$

Expanding Eq. (A.4) in the regions *i*) $k_\perp^2 \leq 4\beta^2$ and *ii*) $k_\perp^2 > 4\beta^2$, we obtain

$$i);\ \int d\rho\rho\big[1 - J_0(\rho k_\perp)\big] K_1(\rho\beta)^2 = \frac{2}{3\beta^2}\frac{k_\perp^2}{4\beta^2} + O\Big(\big(\frac{k_\perp^2}{4\beta^2}\big)^2\Big), \tag{A.5}$$

$$ii);\ \int d\rho\rho\big[1 - J_0(\rho k_\perp)\big] K_1(\rho\beta)^2 = \frac{1}{2\beta^2}\Big[\ell n\Big(\frac{k_\perp^2}{4\beta^2}\Big) + \frac{1}{3}\Big] + O\Big(\frac{4\beta^2}{k_\perp^2}\Big). \tag{A.6}$$

Substituting Eqs. (A.2) and (A.3) in the scalar cross section, Eq. (3.9), and Eqs. (A.5) and (A.6) in the transverse cross section, Eq. (3.10), yields Eq. (3.15) and (3.17), and (3.16) and (3.18), respectively.

REFERENCES

[1] P. A. M. Dirac, Rev. Mod. Phys. 21 (1949), 392.

[2] R. D. Feynman and R. D. Field , Phys. Rev. D15 (1977) 2590;
M. Burkardt and R. Busch, SLAC-PUB-5426, 1991;
S. J. Brodsky and I. A. Schmidt, Phys. Rev. D43 (1991), 179.

[3] P. V. Landshoff, J. C. Polkinghorne and R. Short, Nucl. Phys. B28 (1971), 225.

[4] B. L. Ioffe, Phys. Lett. 30B (1969), 123;
J. Pestieau, P. Roy and H. Terazawa, Phys. Rev. Lett. 25 (1970), 402;
A. Suri and D. R. Yennie, Ann. Phys. 72 (1972), 243.

[5] R. J. Glauber, in "Lectures in Theoretical Physics", Vol. 1, ed. W. E. Brittin and L. G. Duham, Intersciences, New York, 1959.

[6] S. J. Brodsky and Hung Jung Lu, Phys. Rev. Lett. 64 (1990), 1342.

[7] L. D. Landau and I. Ya. Pomeranchuk, Dokl. Akad. Nauk. SSSR 92 (1953), 535, 735;
I. Ya. Pomeranchuk and E. L. Feinberg, Dokl. Akad. Nauk. SSSR 93 (1953), 439.

[8] G. T. Bodwin, S. J. Brodsky, G. P. Lepage, Phys. Rev. D39 (1989), 3287.

[9] J. D. Bjorken, J. B. Kogut and D. E. Soper, Phys. Rev. D3 (1971), 1382

[10] N. N. Nikolaev and B. G. Zakharov, Z. Phys. C49 (1991), 607

[11] S. J. Brodsky, R. Roskies and R. Suaya, Phys. Rev. D8 (1973), 4574.

[12] EMC, J. J. Aubert et al., Phys. Lett. B218 (1989), 248.

[13] I. S. Gradshteyn and I.M. Ryzhik, Table of Integrals, Series and Products, Academic Press 1980.

FIGURE CAPTIONS

1) DIS in the infinite momentum frame.

2) Time-ordered contributions to DIS in the target rest frame.

3) Bethe-Heitler pair production processes in DIS.

4) DIS in a nuclear target in the target rest frame.

5) DIS in covariant perturbation theory.

6) Photon exchange in the t-channel in the Coulomb-photon approximation, in time-ordered perturbation theory.

7) Kinematic regions in the integral over the impact parameter.

8) The curves show the leading-log contributions to the scalar and transverse photo-absorption cross sections $Q^2\sigma$ from Table 1 at $x_{bj} = 0.084$. The circled (squared) dots represent Monte Carlo numerical integrations of the exact transverse (scalar) cross section. The curves and points are normalized to their respective values at $Q^2 = 76GeV^2$. The size of the errors on the Monte Carlo integrations is about 10%.

9) The horizontal lines are the leading-log predictions from Eq. (4.13) and (4.14) for the square root of the mean-square Ioffe time times $x_{bj}M$. The circled (squared) dots represent Monte Carlo numerical integrations of the exact transverse (scalar) Ioffe time times $x_{bj}M$, at x_{bj}= 0.084. The size of the errors on the Monte Carlo integrations is about 10%.

10) The square root of the mean-square Ioffe time times $x_{bj}M$ is plot as function of α. The whole range of α is shown in Fig. a), whereas in Fig. b) the soft quark region is resolved. As in Fig. 8, we take $k_z \simeq 2x_{bj}M$.

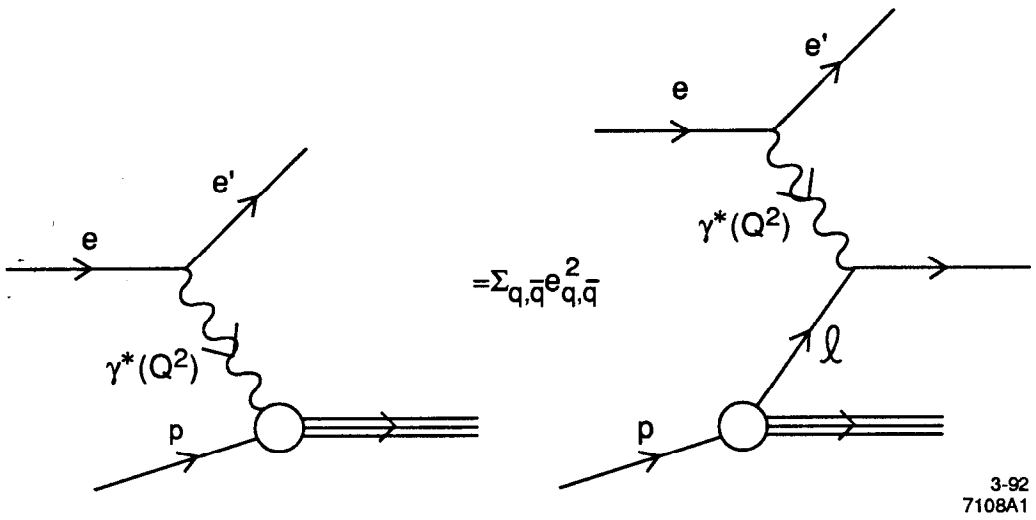

Fig. 1

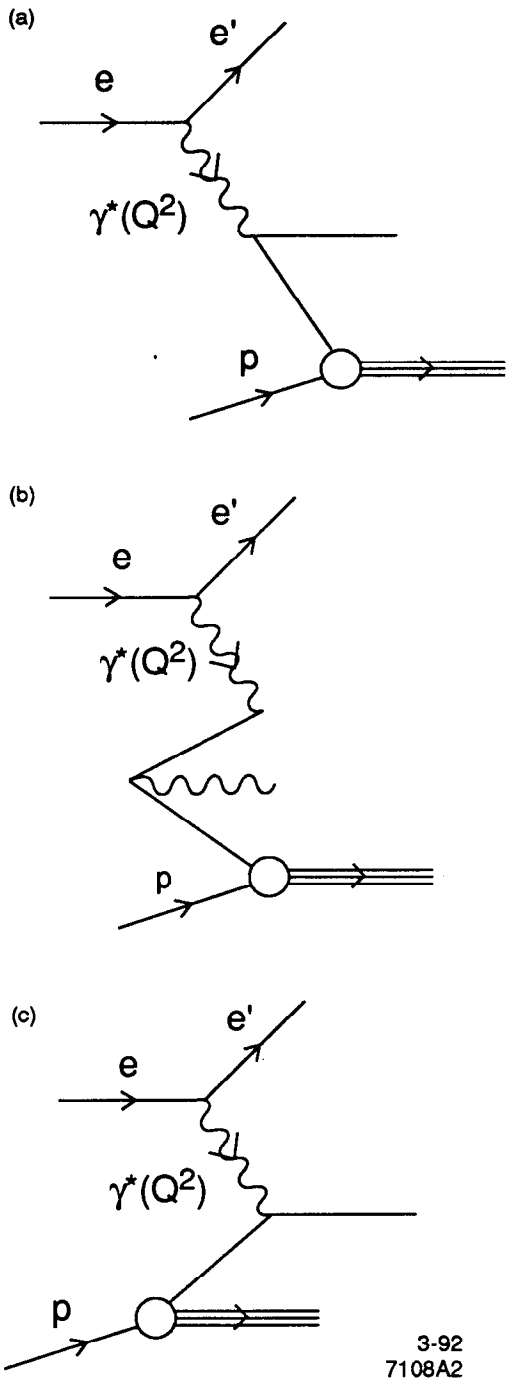

Fig. 2

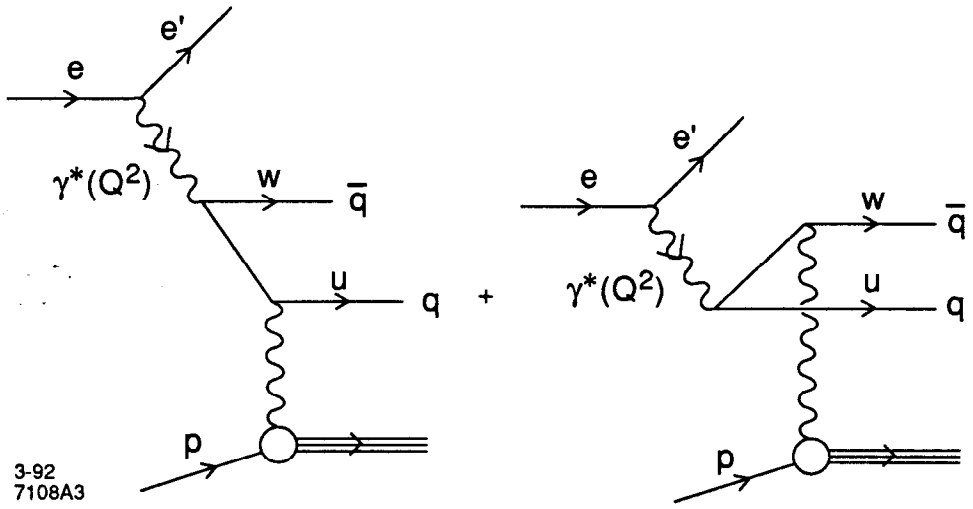

Fig. 3

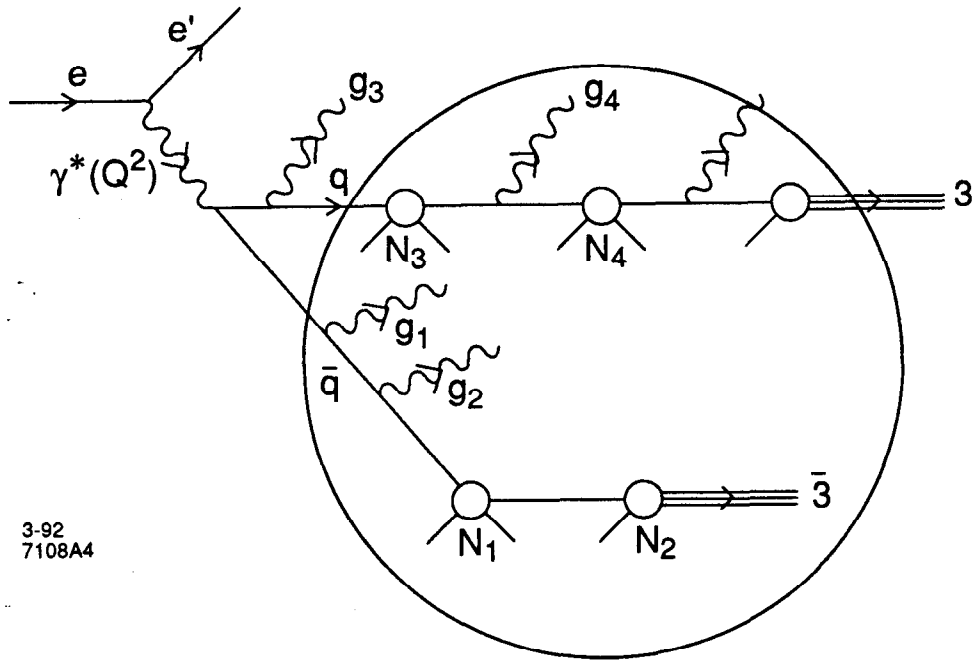

Fig. 4

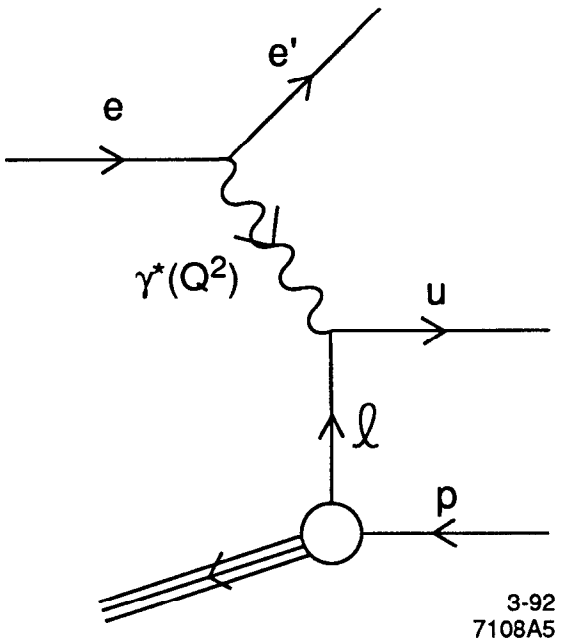

Fig. 5

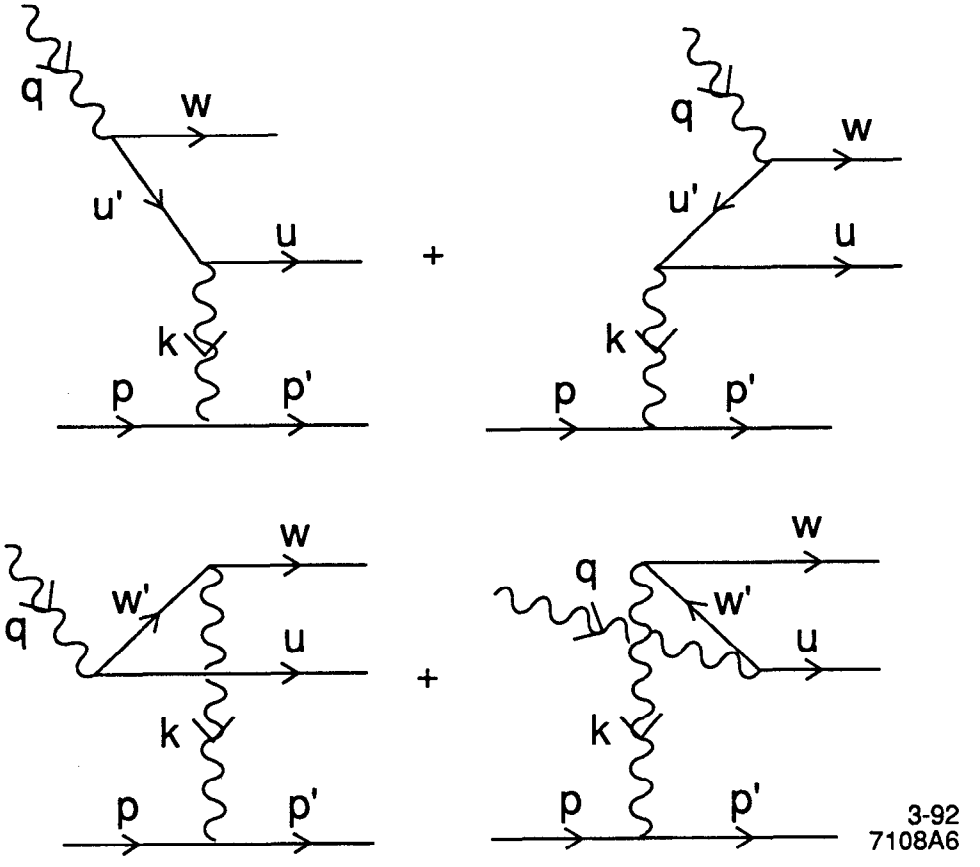

Fig. 6

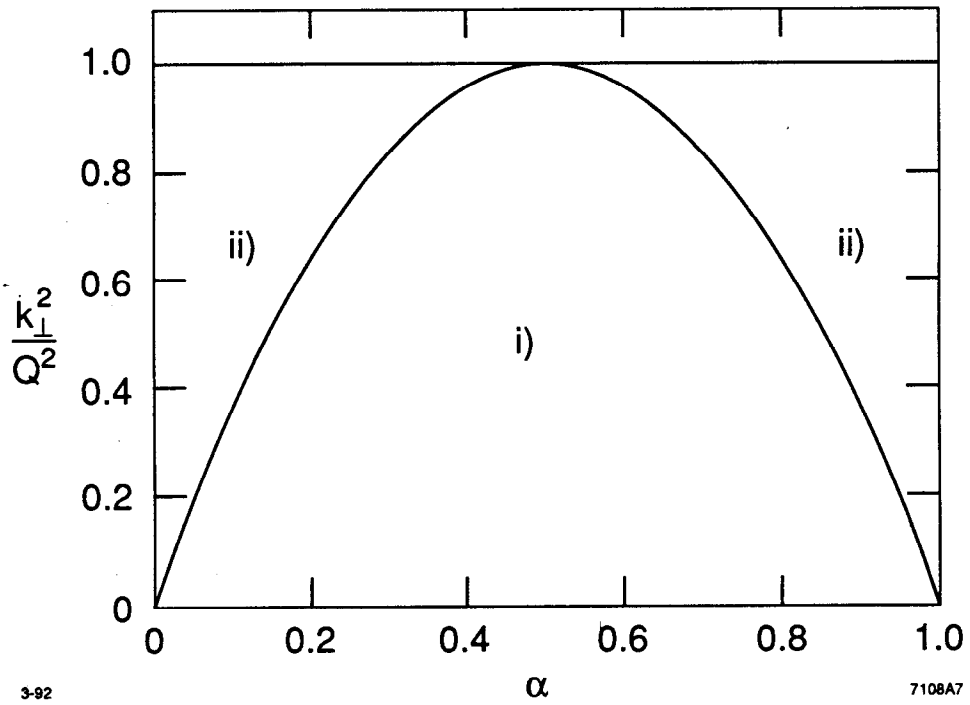

Fig. 7

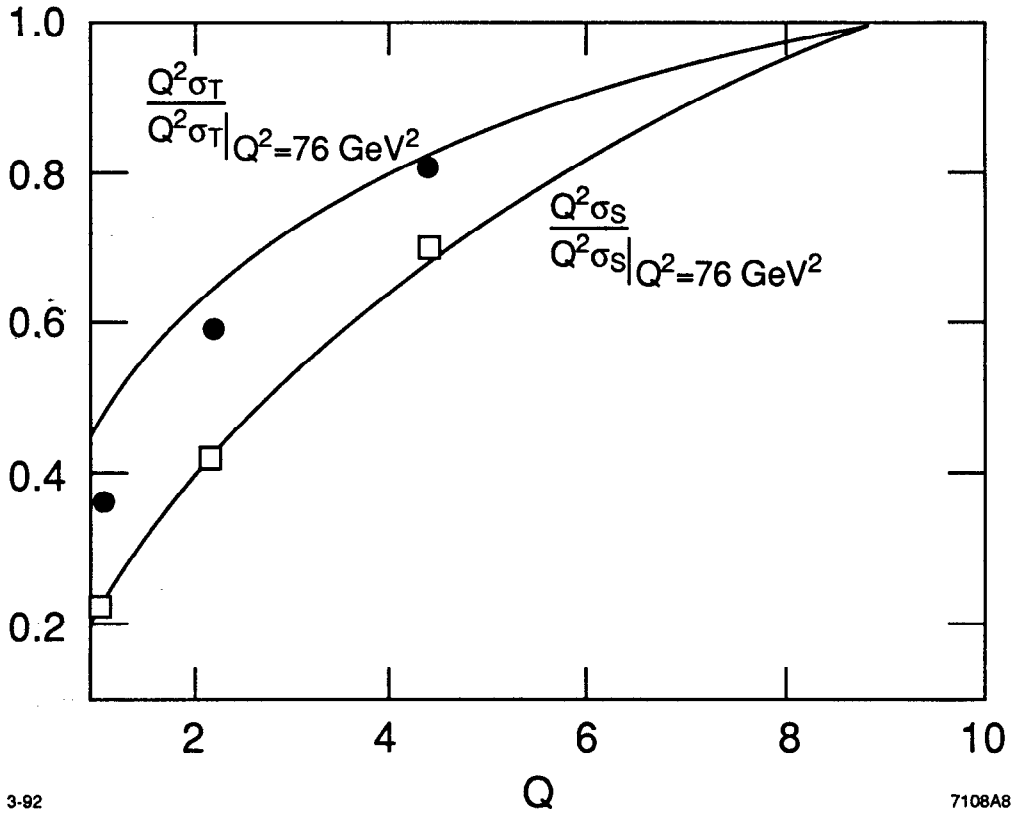
1.0
0.8
0.6
0.4
0.2
$\frac{Q^2\sigma_T}{Q^2\sigma_T|_{Q^2=76\ GeV^2}}$
$\frac{Q^2\sigma_S}{Q^2\sigma_S|_{Q^2=76\ GeV^2}}$
2
4
6
8
10
Q
3-92
7108A8

Fig. 8

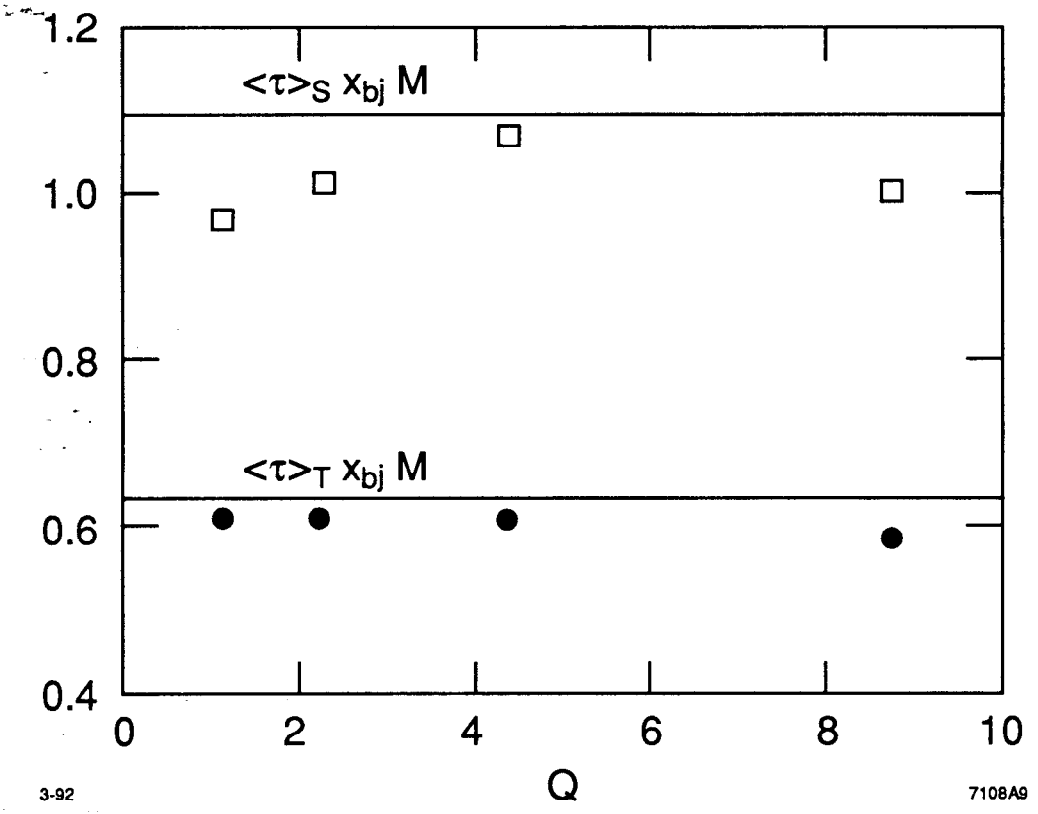

Fig. 9

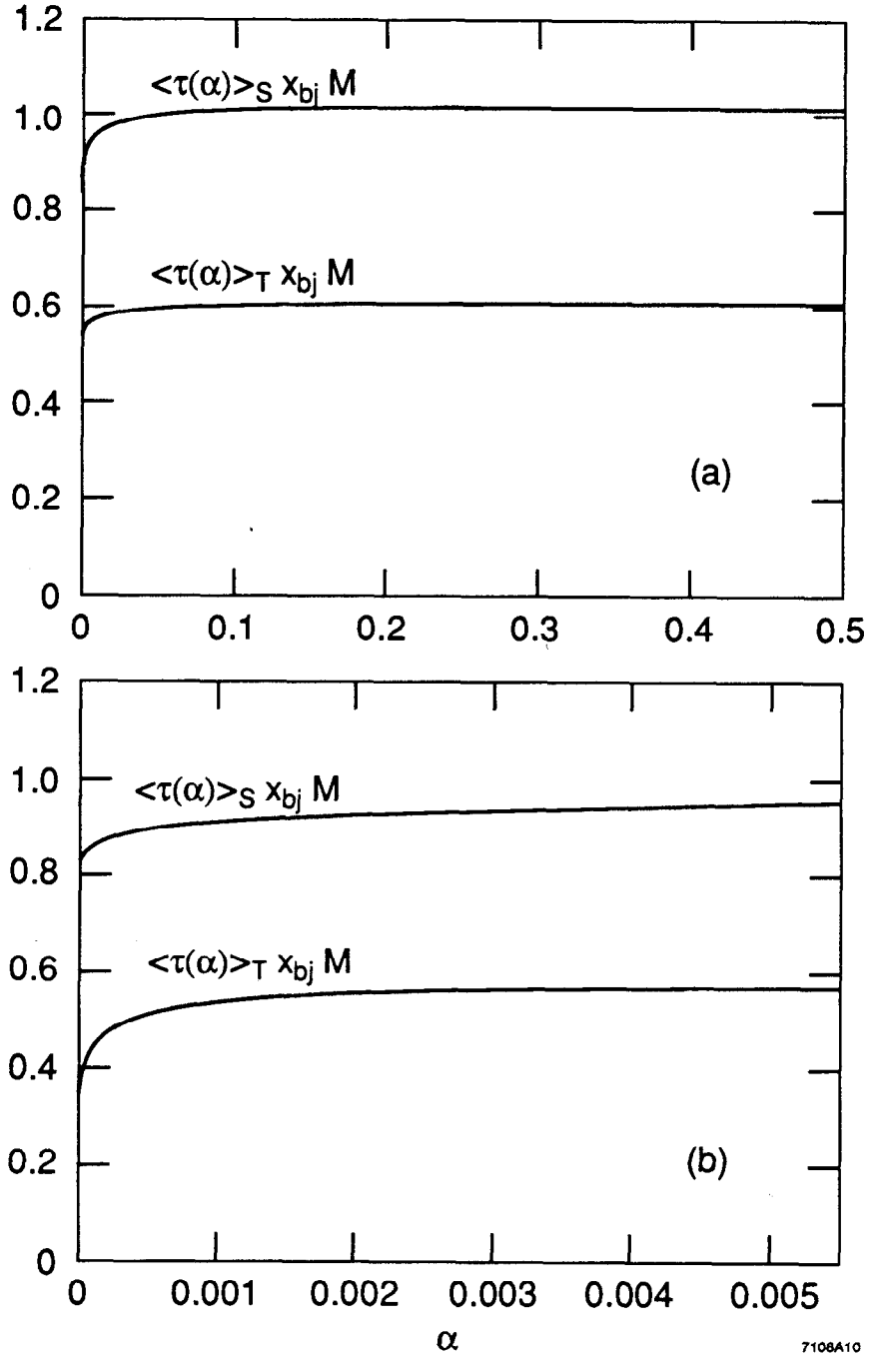
1.2
1.0
0.8
0.6
0.4
0.2
0
<τ(α)>S xbj M
<τ(α)>T xbj M
(a)
0
0.1
0.2
0.3
0.4
0.5
1.2
1.0
0.8
0.6
0.4
0.2
0
<τ(α)>S xbj M
<τ(α)>T xbj M
(b)
0
0.001
0.002
0.003
0.004
0.005
α
3-92
7108A10

Fig. 10